Click-Chemistry-Based Biomimetic Ligands Efficiently Capture G-Quadruplexes In Vitro and Help Localize Them at DNA Damage Sites in Human Cells

Francesco Rota Sperti, Baptiste Dupouy, Jérémie Mitteaux, Angélique Pipier, Marc Pirrotta, Nicolas Chéron, Ibai E. Valverde, David Monchaud

JACS Au
AN OPEN ACCESS JOURNAL OF THE AMERICAN CHEMICAL SOCIETY

pubs.acs.org/jacsau

Letter

Click-Chemistry-Based Biomimetic Ligands Efficiently Capture G-Quadruplexes *In Vitro* and Help Localize Them at DNA Damage Sites in Human Cells

Francesco Rota Sperti, Baptiste Dupouy, Jérémie Mitteaux, Angélique Pipier, Marc Pirrotta, Nicolas Chéron, Ibai E. Valverde,* and David Monchaud*

Cite This: *JACS Au* 2022, 2, 1588–1595

Read Online

ACCESS | Metrics & More | Article Recommendations | Supporting Information

ABSTRACT: Interrogating G-quadruplex (G4) biology at its deepest roots in human cells relies on the design, synthesis, and use of ever smarter molecular tools. Here, we demonstrate the versatility of biomimetic G4 ligands referred to as TASQ (template assembled synthetic G-quartet) in which a biotin handle was incorporated for G4-focused chemical biology investigations. We have rethought the biotinylated TASQ design to make it readily chemically accessible via an efficient click-chemistry-based strategy. The resulting biotinylated, triazole-assembled TASQ, or Bio-TriazoTASQ, was thus shown to efficiently isolate both DNA and RNA G4s from solution by affinity purification protocols, for identification purposes. Its versatility was then further demonstrated by optical imaging that provided unique mechanistic insights into the actual strategic relevance of G4-targeting strategies, showing that ligand-stabilized G4 sites colocalize with and, thus, are responsible for DNA damage foci in human cells.

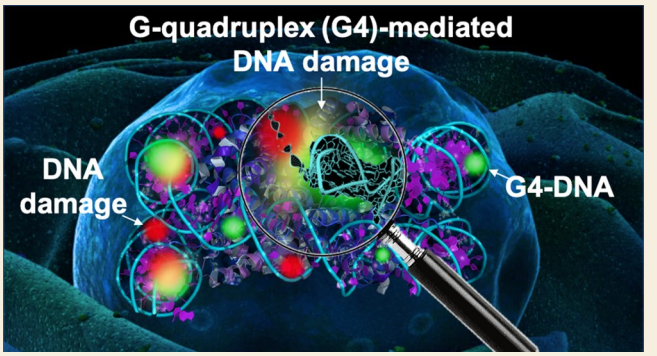

KEYWORDS: *G-quadruplex, ligands, DNA damage, affinity capture, optical imaging*

The synthesis of molecular tools to interrogate G-quadruplex (G4) biology in human cells is an active field of research.[1] Biotinylated probes occupy a central position in chemical biology, as their biotin handle allows for easy isolation of their cellular partners *via ad hoc* avidin-based purification protocols.[2] It is therefore not surprising that biotinylated G4 ligands were soon developed as molecular bait to fish out and identify G4s from human cells: a biotinylated pyridostatin (PDS) was used to pull down telomeric G4s from human fibrosarcoma HT1080 cells prior to their identification by qPCR.[3] A biotinylated pyridodicarboxamide (PDC) was used for *in vitro* selection of G4-forming sequences (among others) within a library of 80 DNA aptamers by SELEX (systematic evolution of ligands by exponential enrichment).[4] This compound also enabled visualization of G4 folding in DNA origami by atomic force microscopy.[5] More recently, a biotinylated perylene diimide (PDI) was used to fish synthetic G4s out of oligonucleotide mixtures in solution.[6]

In these examples, PDS, PDC, and PDI were selected for their established affinity and selectivity for G4s and then chemically modified with a biotin appendage. We recently reported on a complementary approach based on the modification of template-assembled synthetic G-quartets (TASQs).[7,8] The structure of these G4 ligands comprises four guanines (Gs) that can assemble into an intramolecular G-quartet (Figure 1A,B). This synthetic quartet is then prone to interact with the external G-quartet of G4s (a "native" G-quartet) according to a biomimetic, like-likes-like interaction.[9] TASQs are smart ligands as their G-quartet is only assembled upon interaction with G4s, which makes them uniquely *actively selective* for their targets.[10] The first biotinylated TASQ, named BioTASQ,[11−13] was used to selectively isolate (or pull down) G4s from cell lysates before their identification by qPCR and sequencing.

We improved the tedious chemical access to BioTASQ in designing BioCyTASQ (Figure 1A).[14] Satisfyingly, these two TASQs displayed similar G4-interacting properties, and the synthesis of BioCyTASQ was more reliable than that of BioTASQ but remained time-consuming. We thus sought an even shorter chemical access: inspired by reports in which G4 ligands, in general,[15] and a synthetic G-quartet, in particular,[16] were assembled by click chemistry, we decided to investigate

Received: February 9, 2022
Revised: April 29, 2022
Accepted: April 29, 2022
Published: June 17, 2022

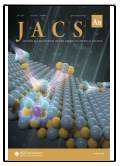

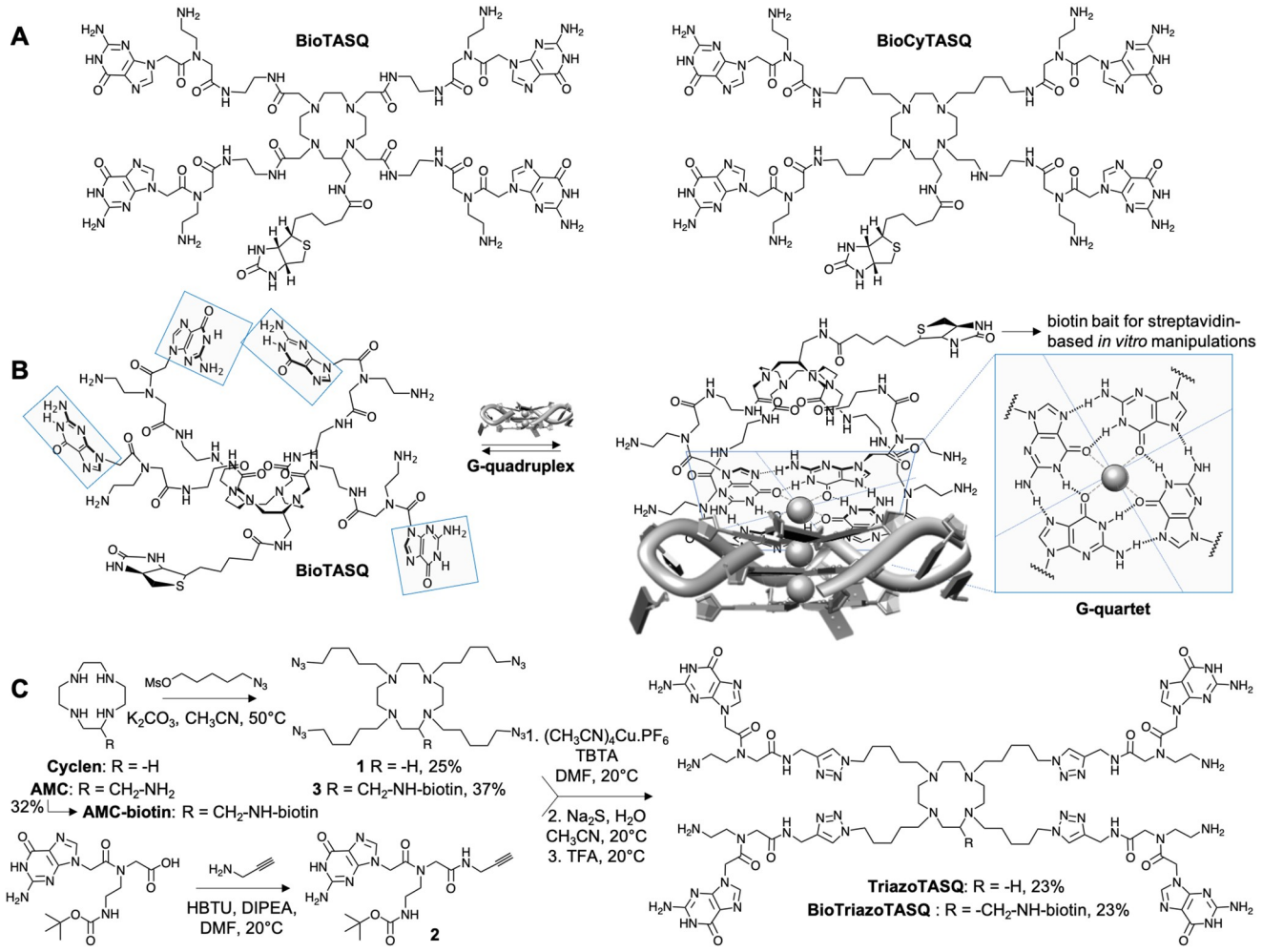

Figure 1. (A) Chemical structure of BioTASQ and BioCyTASQ. (B) Schematic representation of the open and closed conformation of BioTASQ. (C) Chemical synthesis of TriazoTASQ and BioTriazoTASQ (see the Supporting Information for details).

the design of new biotinylated TASQs. This was further motivated by the description of possible beneficial effects of the triazole rings on the G-quartet stability, further discussed hereafter.[16] We thus report here on two clicked TASQs, TriazoTASQ and its biotinylated counterpart BioTriazoTASQ (Figure 1C), for which syntheses are indeed temporally improved by click chemistry as compared to CyTASQ and BioCyTASQ, respectively, with an overall similar efficiency. We then used the latter to visualize G4s by a cellular imaging method referred to as pretargeted G4 imaging and to provide insights into the ability of ligand-stabilized G4s to trigger genetic instability, uniquely colocalizing G4 and DNA damage sites in human cells by a combination of optical detection techniques.

Design, Synthesis, and Evaluations of TriazoTASQ

The design of TASQs was rethought using the copper(I)-catalyzed azide−alkyne cycloaddition (CuAAC) of an alkynylated ^{PNA}G derivative with an azido-substituted cyclen template. This reaction, initially developed by Meldal *et al.*[17] and Sharpless *et al.*[18] and now commonly referred to as click chemistry, enables the coupling of two reagents through the formation of a 1,4-disubstituted-1,2,3-triazole. In our hands, the applicability of CuAAC was first checked with a derivative of the commercially available cyclen, which led to TriazoTASQ (Figure 1C).

This nonbiotinylated TriazoTASQ was synthesized to both validate this novel chemical pathway and assess whether these important structural modifications affect the G4-interacting properties of the resulting TASQ. 5-Azidopentyl mesylate, previously prepared in two steps from the commercially available 5-aminopentan-1-ol in a 42% chemical yield, was reacted with cyclen to afford the azido-substituted cyclen **1** with 25% yield (Supporting Information, Figures S1−S7). The alkynylated ^{PNA}G **2** was prepared from the commercially available Boc-^{PNA}G-OH with 47% yield. After optimization (detailed in Figure S1), these two reagents were then coupled using tetrakis(acetonitrile)copper(I) hexafluorophosphate ($(CH_3CN)_4CuPF_6$) as the copper source and tris[(1-benzyl-1*H*-1,2,3-triazol-4-yl)methyl]amine (TBTA) used as a copper-(I) chelator to afford the $(Boc)_4$TriazoTASQ.Cu(II) complex with 23% yield. It is noteworthy that the cyclen was found to efficiently chelate copper in these conditions, requiring the use of an excess (1.5 mol equiv) of copper salt. After demetalation with sodium sulfide (Na_2S, quantitative yield)[19] and deprotection of the Boc groups with trifluoroacetic acid (TFA, quantitative yield), TriazoTASQ was obtained in a satisfactory chemical yield (2% yield over the longest, six-step branch of the convergent synthesis; 11% yield over the shortest, four-step branch, Figures S2−S7).

https://doi.org/10.1021/jacsau.2c00082
JACS Au 2022, 2, 1588−1595

Table 1. Non-, Mono-, and Dual-Labeled Oligonucleotides Used in This Study

experiment	nature	name	sequence
FRET-melting assay	DNA	F21T	FAM-d[$^{5'}$GGGTTAGGGTTAGGGTTAGGG$^{3'}$]-TAMRA
		F-Myc-T	FAM-d[$^{5'}$GAGGGTGGGGAGGGTGGGGAAG$^{3'}$]-TAMRA
		F-duplex-T	FAM-d[$^{5'}$TATAGCTATATTTTTTTATAGCTATA$^{3'}$]-TAMRA
		ds17 (comp.)	*strand 1*: d[$^{5'}$CCAGTTCGTAGTAACCC$^{3'}$]
			strand 2: d[$^{5'}$GGGTTACTACGAACTGG$^{3'}$]
	RNA	F-TERRA-T	FAM-r[$^{5'}$GGGUUAGGGUUAGGGUUAGGG$^{3'}$]-TAMRA
		F-NRAS-T	FAM-r[$^{5'}$GGGAGGGGCGGGUCUGGG$^{3'}$]-TAMRA
fluorescence pull-down assay	DNA	F-22AG	FAM-d[$^{5'}$AGGGTTAGGGTTAGGGTTAGGG$^{3'}$]
		F-Myc	FAM-d[$^{5'}$GAGGGTGGGGAGGGTGGGGAAG$^{3'}$]
		F-duplex	FAM-d[$^{5'}$TATAGCTATATTTTTTTATAGCTATA$^{3'}$]
	RNA	F-TERRA	FAM-r[$^{5'}$GGGUUAGGGUUAGGGUUAGGG$^{3'}$]
		F-NRAS	FAM-r[$^{5'}$ GGGAGGGGCGGGUCUGGG $^{3'}$]

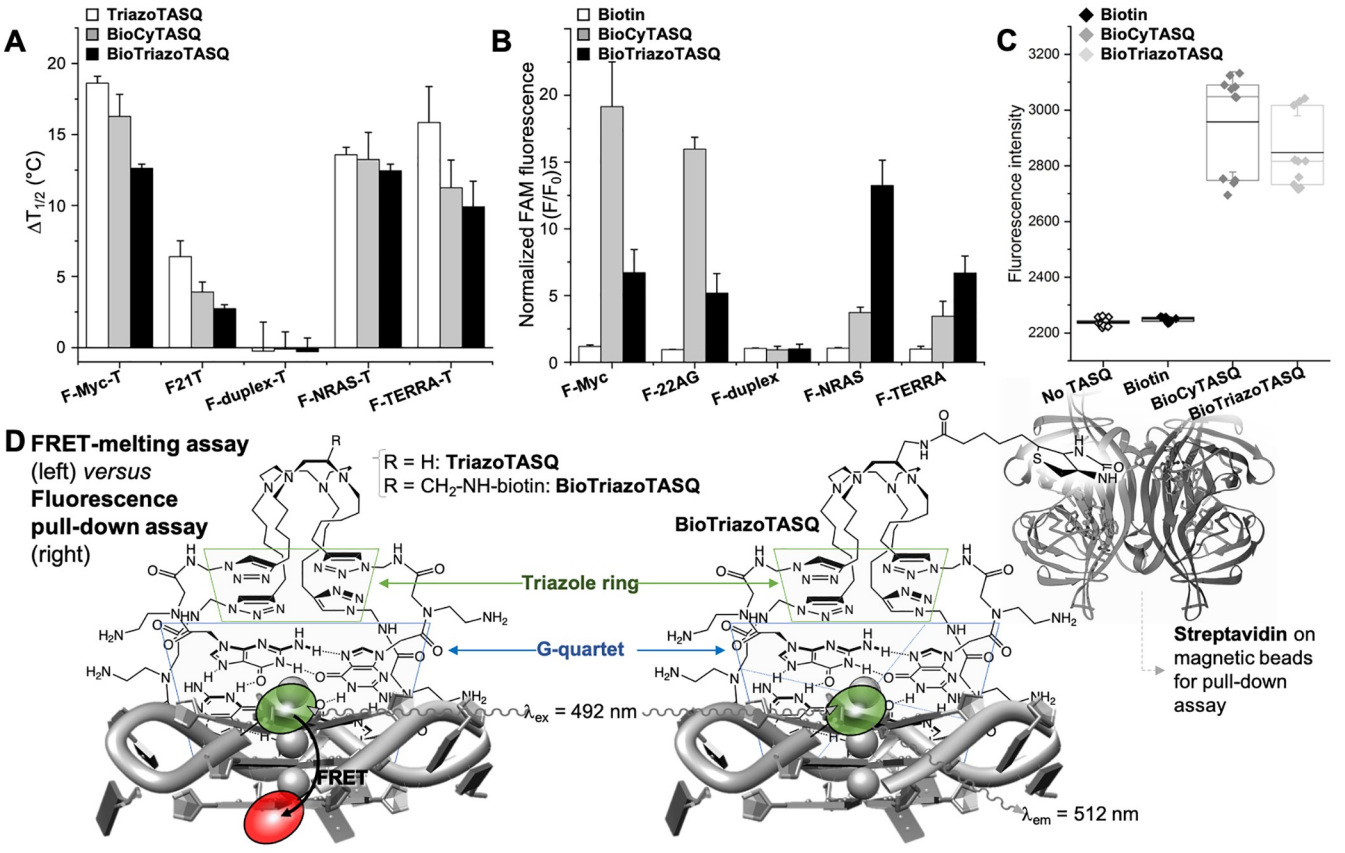

Figure 2. (A) FRET-melting results ($\Delta T_{1/2}$, °C, n = 3) for experiments performed with TriazoTASQ, BioCyTASQ, and BioTriazoTASQ (1 μM, 5 mol equiv) and the G4-DNA F-Myc-T and F21T, the G4-RNA F-NRAS-T and F-TERRA-T, and the control F-duplex-T (0.2 μM). (B) Fluorescence pull-down results (FAM fluorescence enhancement, fold-change, n = 3) for experiments performed with biotin, BioCyTASQ, and BioTriazoTASQ (10 μM, 10 mol equiv) and the G4-DNA F-Myc and F-22AG, the G4-RNA F-NRAS and F-TERRA, and the control F-duplex (1 μM). (C) qPCR pull-down results (SYBR green fluorescence intensity, n = 3) for experiments performed without molecule (control) or with biotin, BioCyTASQ, and BioTriazoTASQ (40 μM, 10 mol equiv) and the G4-strand (4 μM). (D) Schematic representation of TriazoTASQs in interaction with G4s used for FRET-melting and pull-down assays.

The apparent affinity of TriazoTASQ for both G4-DNA and -RNA was evaluated by Förster resonance energy transfer (FRET)-melting assay using biologically relevant G4-forming sequences (Table 1):[20] the G-rich DNA sequences found in the promoter regions of Myc gene (F-Myc-T)[21] and at the human telomeres (F21T);[22] the G-rich RNA sequences found in the 5′-UTR (untranslated region) of the human neuroblastoma RAS oncogene mRNA (F-NRAS-T) and of the human telomeric transcript (F-TERRA-T);[23,24] along with a duplex-forming sequence (F-duplex-T) as control. As seen in Figure 2A and Table 2, these results showed that the extra G4 thermal stability induced by TriazoTASQ (expressed as an increase of the midtransition temperature, $\Delta T_{1/2}$, in °C) was improved as compared to that induced by the parent compound CyTASQ (+23 to +209%). These results were thus in line with the positive effect of the presence of a ring of four triazoles in the close proximity to the synthetic G-quartet described with RAFT-based TASQ.[16] Both TriazoTASQ and CyTASQ were found to be equally selective over duplex-DNA, as demonstrated by the lack of interaction with F-duplex-T

https://doi.org/10.1021/jacsau.2c00082
JACS Au 2022, 2, 1588−1595

Table 2. Results of FRET-Melting and Pull-Down Assays Performed with TASQs

	FRET-melting assay ($\Delta T_{1/2}$, °C)				
	G4-DNA		duplex-DNA	G4-RNA	
	F-Myc-T	F21T	F-duplex-T	F-NRAS-T	F-TERRA-T
CyTASQ[a]	8.7 ± 0.7	5.2 ± 0.4	0.1 ± 0.1	4.4 ± 0.4	10.0 ± 0.1
TriazoTASQ	18.6 ± 0.5	6.4 ± 1.1	−0.2 ± 2.0	13.6 ± 0.5	15.8 ± 2.5
BioCyTASQ	16.3 ± 1.5	3.9 ± 0.7	−0.1 ± 1.2	13.2 ± 1.9	11.2 ± 1.9
BioTriazoTASQ	12.6 ± 0.3	2.7 ± 0.3	−0.2 ± 0.9	12.4 ± 0.4	9.9 ± 1.8
	fluorescence pull-down assay (change in FAM fluorescence intensity, normalized to control)				
	G4-DNA		duplex-DNA	G4-RNA	
	F-Myc	F22AG	F-duplex	F-NRAS	F-TERRA
biotin	1.2 ± 0.1	0.9 ± 0.1	1.0 ± 0.1	1.0 ± 0.1	0.9 ± 0.2
BioCyTASQ	19.1 ± 3.3	15.9 ± 0.9	0.9 ± 0.3	3.7 ± 0.4	3.4 ± 1.1
BioTriazoTASQ	6.7 ± 1.7	5.2 ± 1.4	1.0 ± 0.3	13.2 ± 1.9	6.7 ± 1.3
	qPCR pull-down assay (SYBR Green fluorescence intensity)				
no TASQ	biotin		BioCyTASQ	BioTriazoTASQ	
2238.9 ± 12	2249.0 ± 8		2957.4 ± 179	2847.2 ± 132	

[a]From ref 14.

($\Delta T_{1/2}$ < 0.1 °C for both TASQs). This was confirmed by competitive FRET-melting experiments performed with an excess (50 mol equiv) of a 17 bp duplex-DNA (ds17, Table 1), with selectivity factors ^{FRET}S (calculated as $^{FRET}S = \Delta T_{1/2(+50\ mol\text{-}equiv\text{-}ds17)}/\Delta T_{1/2(no\text{-}competitor)}$) of 0.77 and 0.87 with F-Myc-T and F-TERRA-T, respectively, where ^{FRET}S tends to 1 with selectively (Figure S14).

Design, Synthesis, and Evaluations of BioTriazoTASQ

With the TriazoTASQ scaffold being validated, we next designed BioTriazoTASQ, for which the synthetic scheme (Figures 1C and S8−S13) was directly inspired by that of TriazoTASQ, starting from the noncommercially available aminomethylcyclene (AMC).[25] This template was first coupled to biotin (32% yield) and then reacted with 5-azidopentyl mesylate as above to afford compound **3** in 37% yield. Next, the CuAAC with **2** afforded the $(Boc)_4$BioTriazoTASQ.Cu(II) complex (23% yield) which was subsequently demetalated (Na_2S, quantitative) and deprotected (TFA, quantitative). BioTriazoTASQ was obtained in a lower overall chemical yield than BioCyTASQ (3% versus 5% yield, respectively, for five steps in both instances) but in a shorter manner (54 h versus 126 h for BioTriazoTASQ and BioCyTASQ, respectively).

As above, the apparent G4 affinity of BioTriazoTASQ was assessed by FRET-melting experiments performed with G4-DNA (F-Myc-T and F21T), G4-RNA (F-NRAS-T and F-TERRA-T), and control F-duplex-T. The G4 stabilization induced by BioTriazoTASQ was decreased as compared to the parent compound BioCyTASQ, more markedly with G4-DNA (−23 and −31%, respectively, Figure 2A, Table 2) than with G4-RNA (−9 to −11%). These results indicated that the presence of the triazoles near the synthetic G-quartet did not further improve G4-binding in the biotinylated series, with the initial G4-stabilizing properties of BioCyTASQ being good and better than that of CyTASQ (with the notable exception of the polymorphic F21T). Satisfyingly, the G4-selectivity of BioTriazoTASQ remained very high ($\Delta T_{1/2}$ < 0 °C with F-duplex-T; ^{FRET}S > 0.87, Figure S14), which thus made it a good candidate for G4 pull-down protocols.

This was first investigated through a fluorescence-based affinity capture protocol developed for BioCyTASQ.[14] Briefly, the oligonucleotides used for FRET-melting assays were used labeled by FAM only (F-Myc, F-22AG, F-duplex, F-NRAS, and F-TERRA, Table 1); these oligonucleotides were incubated (1 μM) for 1.5 h at room temperature with either BioCyTASQ or BioTriazoTASQ (10 μM, along with biotin as a control) in the presence of streptavidin-coated magnetic beads. Then, the complexes of nucleic acids/TASQ/beads were magnetically immobilized, the supernatant removed, and the FAM-labeled DNA/RNA was resuspended in solution after a thermal denaturation step (8 min at 90 °C). The capture efficiency of the two TASQs was quantified by the FAM emission of the resulting solution (normalized to the control performed without TASQ).

As seen in Figure 2B and Table 2, both BioCyTASQ and BioTriazoTASQ efficiently capture G4s albeit with a noticeable discrepancy, as BioCyTASQ was found more efficient with G4-DNA (*ca.* 19 and 16-fold enrichment with F-Myc and F-22AG, respectively, *versus ca.* 7- and 5-fold for BioTriazoTASQ) while BioTriazoTASQ was more efficient with G4-RNA (*ca.* 13- and 7-fold enrichment with F-NRAS and F-TERRA, *versus ca.* 4- and 3-fold for BioCyTASQ, a trend confirmed with another G4-RNA, F-TRF2, Figure S15). One hypothesis to explain the preferential interaction of BioTriazoTASQ with G4-RNA could be that the stacking interaction between the triazole ring and the intramolecular G-quartet brings them closer and pushes the connecting linkers outward. This would make the TASQ's quartet more sterically demanding, which thus could drive the interaction toward G4-RNA, as their external G-quartet is more accessible than that of the G4-DNA. To investigate this, a series of molecular dynamics (MD) simulations were undertaken with CyTASQ and TriazoTASQ (Figure S16): these calculations did not confirm the coplanar assembly of the triazoles but indicated that (i) TriazoTASQ is more sterically demanding than CyTASQ (solvent-accessible surface area = 21.4 versus 18.5 nm^2) and (ii) the nature of the guanine arms does influence the steric hindrance of external G-quartet, with that of CyTASQ being hindered by surrounding amide connectors while that of TriazoTASQ being more freely accessible (further discussed in the Supporting Information). These subtle differences might thus be responsible for the differential recognition of DNA/RNA G4s. Finally, both TASQs were enticingly selective, as none of them captured

https://doi.org/10.1021/jacsau.2c00082
JACS Au 2022, 2, 1588−1595

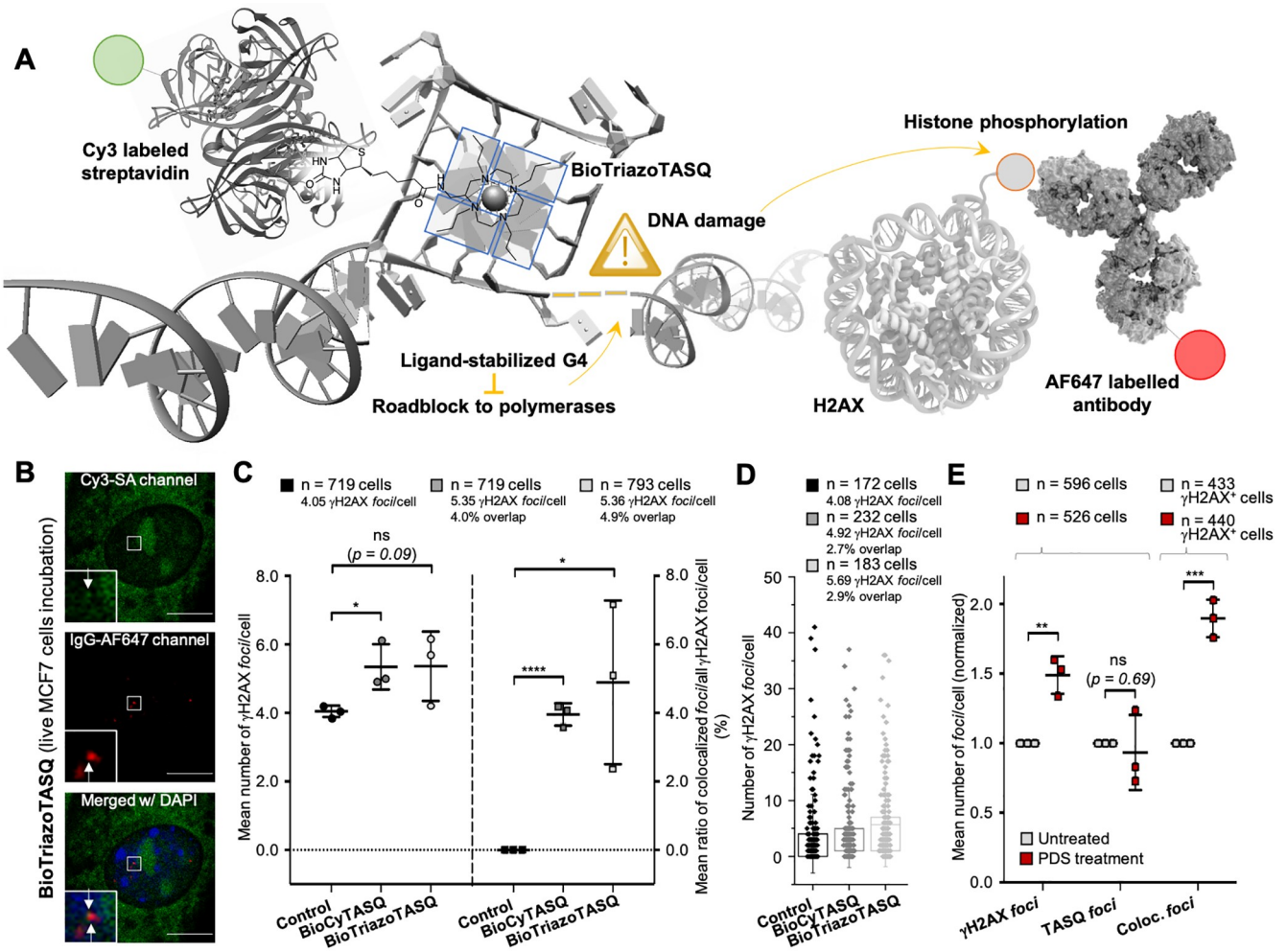

Figure 3. (A) Schematic representation of the TASQ-stabilized G4-mediated DNA damage and related signaling pathway used to colocalize G4 and DNA damage sites (of note, the primary, anti-γH2AX antibody is removed for clarity). (B) High-resolution optical images of MCF7 cells treated with BioTriazoTASQ (1 μM, 24 h), tagged with Cy3-SA (green) after cell fixation (scale bar = 10 μm), which is followed by immunodetection of DNA damage *foci* (γH2AX, red) and chromatin staining by DAPI (blue). Inset and arrows highlight of the nucleoplasmic sites where both DSBs and TASQ colocalize. (C,D) Automated (C) or manual (D) quantification of γH2AX *foci*/cell, with or without TASQ treatment, and of the overlaps between green (TASQ) and red signals (γH2AX). (E) Modulation of the γH2AX, BioTriazoTASQ and common *foci* upon incubation of MCF7 cells by PDS (5 μM, 6 h) and G4-labeling by BioTriazoTASQ (used after cell fixation; 10 μM, overnight) and Cy3-SA. Statistics: *p*-values, $*p < 0.05$, $**p < 0.01$, and $***p < 0.001$.

F-duplex, which was further confirmed by competitive experiments performed with an excess (25 mol equiv) of a nucleic acid mixture (calf thymus DNA, or CT-DNA), with selectivity factor $S > 0.94$ (Figure S15).

To go a step further, we investigated the G4-capturing ability of both TASQs in more biologically relevant conditions. To this end, we incorporated a G4-forming sequence into a long DNA strand (97-nt long, $d[N_{41}\text{-}G_3(CAG_3)_3\text{-}N_{38}]$),[26] devoid of fluorescent tags, which made its detection possible only through qPCR analysis. This new protocol was performed with BioCyTASQ and BioTriazoTASQ (Figure 2C), along with two control experiments performed without TASQ (for the nonspecific binding of oligonucleotides on beads) and with biotin. The protocol thus comprised an incubation of the DNA (4 μM) without or with TASQ/biotin (40 μM, 10 mol equiv) in the presence of the streptavidin-coated magnetic beads for 2 h at room temperature, followed by magnetic immobilization of DNA/TASQ/beads and release of captured DNA (thermal denaturation) prior to qPCR amplification (expressed as SYBR Green fluorescence intensity, or FI). In these conditions, both BioCyTASQ and BioTriazoTASQ showed good efficiency to capture G4 (ΔFI = 718.4 and 608.3, respectively, when compared to the experiment performed without TASQ, Figure 2C), thus confirming their suitability for being used as molecular bait for G4s embedded in long nucleic acid sequences.

Pretargeted Optical Imaging Reveals G4-Mediated DNA Damage Sites

We already showed that biotinylated TASQs can also be used to track and detect G4s in human cells due to a pretargeted imaging protocol using the fluorescently labeled streptavidin Cy3-SA (schematically represented in Figures 3A).[14] To go a step further, we decided to implement this protocol to demonstrate that G4s can act as roadblocks to polymerases, thereby creating a crisis situation recognized as a DNA damage.[27,28] The propensity of G4s to trigger DNA damage when stabilized by ligands such as PDS and CX-5461 is firmly documented.[29−32] This is commonly shown by a G4 ligand-promoted increase in antibody labeling the most lethal form of

https://doi.org/10.1021/jacsau.2c00082
JACS Au 2022, 2, 1588−1595

DNA damage, the double strand breaks (DSBs), by either the phosphorylated histone γH2AX[33,34] or tumor suppressor p53 binding protein 1 (53BP1).[35] Direct demonstrations of the colocalization of G4 and DNA damage sites are sparse in the literature, including the concomitant immunodetection of DSBs and G4s using the G4-specific BG4[36] in combination anti-γH2AX (upon incubation with PDS)[37] or anti-53BP1 antibodies (incubation with CM03),[38] and a combination of the anti-G4 1H6[39] with anti-γH2AX (incubation with PDS)[40] or anti-53BP1 antibodies (incubation with EMICORON).[41] While most of these observations were qualitative in nature, Neidle *et al.* provided a quantitative analysis of the BG4/anti-53BP1 colocalization,[38] showing that 1.4% of the BG4 *foci* (*ca.* 400 *foci*/nucleus) were associated with DNA damage (*ca.* 20 53BP1 *foci*/nucleus).

Surprisingly, examples of the concomitant use of a G4 probe and a DNA damage marker are even sparser, chiefly, a qualitative example involving a combination of a naphthalene diimide (NDI) and anti-γH2AX antibody.[42] To provide a quantitative analysis, we treated MCF7 cells with either BioCyTASQ or BioTriazoTASQ (1 μM, 24 h; IC_{50} > 100 μM) before fixation with cold MeOH (5 min) followed by cell permeabilization and sequential incubation (in a dark chamber) with SA-Cy3 (1 μg/mL, 1 h), γH2AX-specific antibody (1/2000, 2 h), fluorophore-labeled secondary antibody (IgG-AF647, 1/500, 45 min) and DAPI (1 μg/mL, 5 min). The collected images (Figures 3B, S17, and S18) indicate first that live incubation of MCF7 cells with a subtoxic concentration of TASQs triggered a slight induction of DNA damage, quantified as the average number of γH2AX *foci* per cell (*ca.* 5.3 *foci*/nucleus for TASQ-treated cells, versus 4.0 *foci*/nucleus for untreated cells, >160 cells/conditions (n = 3), Figures 3C).

To make this analysis straightforward and reliable, we developed an automated image processing FIJI macro for foci quantification (the script is provided in the Supporting Information, and the macro is downloadable). This analysis led to the quantification of colocalized Cy3-SA-tagged TASQ and γH2AX sites, with approximately 4.0 and 4.9% of the BioCyTASQ- and BioTriazoTASQ-labeled foci overlapping with γH2AX foci (insets in Figure 3B; Figure 3C). The reliability and accuracy of the automatic scoring was verified by manual scoring (on *ca.* 30% of the samples, *i.e.*, 600 cells analyzed): it was found that 2.7 and 2.9% of the BioCyTASQ- and BioTriazoTASQ-labeled foci overlapped with γH2AX foci (Figure 3D), which is yet lower than that of the automatized count (which depends on the number of analyzed cells but also on the selected thresholds) but in a close range. Globally, these low percentages originate in the weak ability of TASQ to induce DNA damage (*ca.* 5 foci/cell, + 33% increase as compared to untreated cells); however, they are higher than the common BG4/53BP1 sites described above, which results from the far lower number of G4 sites detected by TASQ (*ca.* 30 foci/nucleus) than by BG4 (*ca.* 400 foci/nucleus, *i.e.*, 23-fold more), which has to be compared to the 4-fold difference (only) in damage site count (*ca.* 5 γH2AX versus 20 53BP1 foci/nucleus). In order to increase the number of DNA damage sites, cells were preincubated with PDS (5 μM, 6 h), which indeed resulted in a raise of the number of γH2AX foci (1.5-fold, Figures 3E and S19). To avoid competition between the two ligands (PDS and TASQ) for the cellular G4 targets, BioTriazoTASQ was used here as a postfixation agent (10 μM, overnight): despite a slight decrease of the number of TASQ foci (0.9-fold), the number of common TASQ/γH2AX foci significantly increased (1.9-fold), which indicates both the suitability of this approach to the study of G4-targeting DNA damaging agents and the versatility of TASQ that can be used either in live cells or after cell fixation. Altogether, these results provided a direct demonstration that ligand-stabilized G4 sites can indeed colocalize with DSBs in cells.

In conclusion, this wealth of data continues to demonstrate the interest of versatile and multivalent molecular tools for chemical biology investigations, in general, and of biomimetic, TASQ-based G4 ligands for G4-focused research, in particular. The biotinylated TASQ used here can indeed be implemented in various *in vitro* manipulations (affinity capture, optical imaging) to sharpen our knowledge about G4 biology. The technicality of TASQs is in considering their chemical access, that we have tried to improve here by using click chemistry for the key conjugation step between the ^{PNA}G units and the cyclen-based template. Overall, this strategy turned out to be synthetically advantageous and also revealed that changes to the TASQ scaffold result in a subtle modification of the G4-interacting properties of the resulting TASQs, as exemplified by the differential ability to pull down G4-DNA (BioCyTASQ) or G4-RNA (BioTriazoTASQ). We are currently further investigating the possible origins of this observation, as many parameters, not easily disentangled (including the molecular volume and flexibility, the accessibility of the external G-quartet), have to be taken into account. However, this empirical observation is important as it may guide the selection of the most suited candidate in our growing portfolio of TASQs as a function of the intended application.

METHODOLOGY

Cell Culture

MCF7 cells were routinely cultured in 75 cm^2 tissue culture flasks at 37 °C in a humidified, 5% CO_2 atmosphere in Dulbecco's modified Eagle's medium (DMEM) supplemented with 10% fetal bovine serum and 1% penicillin−streptomycin (5.0 U mL^{-1} pen/5.0 μg mL^{-1}) mixture. Cells were subcultured twice a week using standard protocols.

Pretargeted G4 Imaging

Round coverslips (12 mm) were sterilized with 70% ethanol before cell seeding. MCF7 cells were seeded at a density of 6 × 10^4 cells per coverslip on chambered coverslips (24-well plate) and allowed to recover overnight. Cells were incubated with either BioCyTASQ or BioTriazoTASQ (1 μM, 24 h) at 37 °C, washed once with PBS 1×, fixed and permeabilized with cold MeOH for 5 min at −20 °C, washed with PBS 1× (3 × 5 min), then incubated with (1) blocking buffer (PBS 1X/BSA 1%/Triton X-100 0.1%, 10 min at 25 °C); (2) streptavidin-Cy3 (ThermoFisher Scientific 434315, 1 μg/mL, 1 h); (3) PBS 1×/Triton X-100 0.1% (3 × 5 min); (4) anti-γH2AX antibody (Merck Millipore 05-636, mouse monoclonal Ab, 1/2000, 2 h in dark chamber); (5) PBS 1×/Triton X-100 0.1% (3 × 5 min); (6) anti-mouse Ig-AF647 antibody (donkey, 1/500, 45 min in dark chamber); (7) PBS 1×/Triton X-100 0.1% (3 × 5 min); (8) DAPI (1 μg/mL, 5 min in dark chamber); and (9) PBS 1× (3 × 5 min). Cells were mounted and imaged with a confocal laser-scanning microscope with a 63× oil objective, collected through the following channels: DAPI (emission 448−475 nm), AF647 (emission 644−696 nm), and Cy3 (emission: 558−575 nm).

https://doi.org/10.1021/jacsau.2c00082
JACS Au 2022, 2, 1588−1595

Image Processing

Images were processed with ImageJ (https://fiji.sc); for statistical hypothesis tests, Student's *t*-test and Welch's unequal variances *t*-test were used depending on variances equality. The automated *foci* quantification was made according to homemade FIJI add-ons, which can be download (free of charge) at https://github.com/ICMUB/TASQ/blob/main/macro-eng_quantif-foci-int_TASQ-gH2AX.ijm

■ ASSOCIATED CONTENT

Supporting Information

The Supporting Information is available free of charge at https://pubs.acs.org/doi/10.1021/jacsau.2c00082.

Synthesis and characterizations of TriazoTASQ and BioTriazoTASQ; protocols and additional results for FRET-melting experiments and pull-down assays; molecular dynamics simulations; pretargeted optical imaging performed without or with PDS pretreatment (PDF)

FIJI add-ons (ZIP)

■ AUTHOR INFORMATION

Corresponding Authors

Ibai E. Valverde − *Institut de Chimie Moléculaire, ICMUB CNRS UMR 6302, UBFC Dijon, 21078 Dijon, France;* orcid.org/0000-0002-5802-4131; Email: ibai.valverde@u-bourgogne.fr

David Monchaud − *Institut de Chimie Moléculaire, ICMUB CNRS UMR 6302, UBFC Dijon, 21078 Dijon, France;* orcid.org/0000-0002-3056-9295; Email: david.monchaud@cnrs.fr

Authors

Francesco Rota Sperti − *Institut de Chimie Moléculaire, ICMUB CNRS UMR 6302, UBFC Dijon, 21078 Dijon, France*

Baptiste Dupouy − *Institut de Chimie Moléculaire, ICMUB CNRS UMR 6302, UBFC Dijon, 21078 Dijon, France*

Jérémie Mitteaux − *Institut de Chimie Moléculaire, ICMUB CNRS UMR 6302, UBFC Dijon, 21078 Dijon, France;* orcid.org/0000-0003-0839-553X

Angélique Pipier − *Institut de Chimie Moléculaire, ICMUB CNRS UMR 6302, UBFC Dijon, 21078 Dijon, France*

Marc Pirrotta − *Institut de Chimie Moléculaire, ICMUB CNRS UMR 6302, UBFC Dijon, 21078 Dijon, France*

Nicolas Chéron − *PASTEUR, Département de chimie, École normale supérieure, PSL University, Sorbonne Université, CNRS, 75005 Paris, France;* orcid.org/0000-0002-4090-5897

Complete contact information is available at: https://pubs.acs.org/10.1021/jacsau.2c00082

Notes

The authors declare no competing financial interest.

■ ACKNOWLEDGMENTS

This work was supported by the CNRS (N.C., I.E.V., and D.M.), iSITE BFC (COMUE UBFC, PIA2, Grant No. UB21018.MUB.IS, for D.M.), and the European Union (PO FEDER-FSE Bourgogne 2014/2020 programs, Grant No. BG0021532 for D.M.). This work was performed using HPC resources from GENCI−IDRIS (Grant 2021-077156). The authors thank Jo Zell for her help in editing the manuscript.

■ REFERENCES

(1) Raguseo, F.; Chowdhury, S.; Minard, A.; Di Antonio, M. Chemical-biology approaches to probe DNA and RNA G-quadruplex structures in the genome. *Chem. Commun.* **2020**, *56*, 1317−1324.

(2) Wilchek, M.; Bayer, E. A. The avidin-biotin complex in bioanalytical applications. *Anal. Biochem.* **1988**, *171*, 1−32.

(3) Mueller, S.; Kumari, S.; Rodriguez, R.; Balasubramanian, S. Small-molecule-mediated G-quadruplex isolation from human cells. *Nat. Chem.* **2010**, *2*, 1095−1098.

(4) Renaud de la Faverie, A.; Hamon, F.; Di Primo, C.; Largy, E.; Dausse, E.; Delauriere, L.; Landras-Guetta, C.; Toulme, J.-J.; Teulade-Fichou, M.-P.; Mergny, J.-L. Nucleic acids targeted to drugs: SELEX against a quadruplex ligand. *Biochimie* **2011**, *93*, 1357−1367.

(5) Rajendran, A.; Endo, M.; Hidaka, K.; Phong Lan Thao, T.; Teulade-Fichou, M.-P.; Mergny, J.-L.; Sugiyama, H. G-quadruplex-binding ligand-induced DNA synapsis inside a DNA origami frame. *RSC Adv.* **2014**, *4*, 6346−6355.

(6) Busto, N.; Calvo, P.; Santolaya, J.; Leal, J. M.; Guédin, A.; Barone, G.; Torroba, T.; Mergny, J.-L.; García, B. Fishing for G-Quadruplexes in Solution with a Perylene Diimide Derivative Labeled with Biotins. *Chem.—Eur. J.* **2018**, *24*, 11292−11296.

(7) Nikan, M.; Sherman, J. C. Template-assembled synthetic G-quartets (TASQs). *Angew. Chem., Int. Ed.* **2008**, *47*, 4900−4902.

(8) Stefan, L.; Monchaud, D. Applications of guanine quartets in nanotechnology and chemical biology. *Nat. Rev. Chem.* **2019**, *3*, 650−668.

(9) Stefan, L.; Guedin, A.; Amrane, S.; Smith, N.; Denat, F.; Mergny, J.-L.; Monchaud, D. DOTASQ as a prototype of nature-inspired G-quadruplex ligand. *Chem. Commun.* **2011**, *47*, 4992−4994.

(10) Haudecoeur, R.; Stefan, L.; Denat, F.; Monchaud, D. A Model of Smart G-Quadruplex Ligand. *J. Am. Chem. Soc.* **2013**, *135*, 550−553.

(11) Yang, S. Y.; Lejault, P.; Chevrier, S.; Boidot, R.; Robertson, A. G.; Wong, J. M.; Monchaud, D. Transcriptome-wide identification of transient RNA G-quadruplexes in human cells. *Nat. Commun.* **2018**, *9*, 4730.

(12) Renard, I.; Grandmougin, M.; Roux, A.; Yang, S. Y.; Lejault, P.; Pirrotta, M.; Wong, J. M. Y.; Monchaud, D. Small-molecule affinity capture of DNA/RNA quadruplexes and their identification in vitro and in vivo through the G4RP protocol. *Nucleic Acids Res.* **2019**, *47*, 5502−5510.

(13) Yang, S. Y.; Monchaud, D.; Wong, J. M. Y. Global mapping of RNA G-quadruplexes (G4-RNAs) using G4RP-seq. *Nat. Protoc.* **2022**, *17*, 870−889.

(14) Rota Sperti, F.; Charbonnier, T.; Lejault, P.; Zell, J.; Bernhard, C.; Valverde, I. E.; Monchaud, D. Biomimetic, Smart, and Multivalent Ligands for G-Quadruplex Isolation and Bioorthogonal Imaging. *ACS Chem. Biol.* **2021**, *16*, 905−914.

(15) Saha, P.; Panda, D.; Dash, J. The application of click chemistry for targeting quadruplex nucleic acids. *Chem. Commun.* **2019**, *55*, 731−750.

(16) Murat, P.; Gennaro, B.; Garcia, J.; Spinelli, N.; Dumy, P.; Defrancq, E. The Use of a Peptidic Scaffold for the Formation of Stable Guanine Tetrads: Control of a H-bonded Pattern in Water. *Chem.—Eur. J.* **2011**, *17*, 5791−5795.

(17) Tornøe, C. W.; Christensen, C.; Meldal, M. Peptidotriazoles on solid phase:[1, 2, 3]-triazoles by regiospecific copper (I)-catalyzed 1, 3-dipolar cycloadditions of terminal alkynes to azides. *J. Org. Chem.* **2002**, *67*, 3057−3064.

(18) Rostovtsev, V. V.; Green, L. G.; Fokin, V. V.; Sharpless, K. B. A Stepwise Huisgen Cycloaddition Process: Copper(I)-Catalyzed Regioselective "Ligation" of Azides and Terminal Alkynes. *Angew. Chem., Int. Ed.* **2002**, *41*, 2596−2599.

(19) Knör, S.; Modlinger, A.; Poethko, T.; Schottelius, M.; Wester, H. J.; Kessler, H. Synthesis of Novel 1, 4, 7, 10-Tetraazacyclodecane-1, 4, 7, 10-Tetraacetic Acid (DOTA) Derivatives for Chemoselective

Attachment to Unprotected Polyfunctionalized Compounds. *Chem.—Eur. J.* **2007**, *13*, 6082−6090.
(20) De Rache, A.; Mergny, J.-L. Assessment of selectivity of G-quadruplex ligands via an optimized FRET melting assay. *Biochimie* **2015**, *115*, 194−202.
(21) Balasubramanian, S.; Hurley, L. H.; Neidle, S. Targeting G-quadruplexes in gene promoters: a novel anticancer strategy? *Nat. Rev. Drug Discovery* **2011**, *10*, 261−275.
(22) Xu, Y. Chemistry in human telomere biology: structure, function and targeting of telomere DNA/RNA. *Chem. Soc. Rev.* **2011**, *40*, 2719−2740.
(23) Bugaut, A.; Balasubramanian, S. 5 '-UTR RNA G-quadruplexes: translation regulation and targeting. *Nucleic Acids Res.* **2012**, *40*, 4727−4741.
(24) Lyu, K.; Chow, E. Y.-C.; Mou, X.; Chan, T.-F.; Kwok, C. K. RNA G-quadruplexes (rG4s): genomics and biological functions. *Nucleic Acids Res.* **2021**, *49*, 5426−5450.
(25) Rousselin, Y.; Sok, N.; Boschetti, F.; Guilard, R.; Denat, F. Efficient Synthesis of New C-Functionalized Macrocyclic Polyamines. *Eur. J. Org. Chem.* **2010**, *2010*, 1688−1693.
(26) Jamroskovic, J.; Obi, I.; Movahedi, A.; Chand, K.; Chorell, E.; Sabouri, N. Identification of putative G-quadruplex DNA structures in S. pombe genome by quantitative PCR stop assay. *DNA Repair* **2019**, *82*, 102678.
(27) Zell, J.; Rota Sperti, F.; Britton, S.; Monchaud, D. DNA folds threaten genetic stability and can be leveraged for chemotherapy. *RSC Chem. Biol.* **2021**, *2*, 47−76.
(28) Puget, N.; Miller, K.; Legube, G. Non-canonical DNA/RNA structures during Transcription-Coupled Double-Strand Break Repair: Roadblocks or Bona fide repair intermediates? *DNA Repair* **2019**, *81*, 102661.
(29) Zimmer, J.; Tacconi, E. M. C.; Folio, C.; Badie, S.; Porru, M.; Klare, K.; Tumiati, M.; Markkanen, E.; Halder, S.; Ryan, A.; Jackson, S. P.; Ramadan, K.; Kuznetsov, S. G.; Biroccio, A.; Sale, J. E.; Tarsounas, M. Targeting BRCA1 and BRCA2 Deficiencies with G-Quadruplex-Interacting Compounds. *Mol. Cell* **2016**, *61*, 449−460.
(30) Xu, H.; Di Antonio, M.; McKinney, S.; Mathew, V.; Ho, B.; O'Neil, N. J.; Santos, N. D.; Silvester, J.; Wei, V.; Garcia, J.; Kabeer, F.; Lai, D.; Soriano, P.; Banáth, J.; Chiu, D. S.; Yap, D.; Le, D. D.; Ye, F. B.; Zhang, A.; Thu, K.; Soong, J.; Lin, S.-c.; Tsai, A. H. C.; Osako, T.; Algara, T.; Saunders, D. N.; Wong, J.; Xian, J.; Bally, M. B.; Brenton, J. D.; Brown, G. W.; Shah, S. P.; Cescon, D.; Mak, T. W.; Caldas, C.; Stirling, P. C.; Hieter, P.; Balasubramanian, S.; Aparicio, S. CX-5461 is a DNA G-quadruplex stabilizer with selective lethality in BRCA1/2 deficient tumours. *Nat. Commun.* **2017**, *8*, 14432.
(31) Bossaert, M.; Pipier, A.; Riou, J.-F.; Noirot, C.; Nguyên, L.-T.; Serre, R.-F.; Bouchez, O.; Defrancq, E.; Calsou, P.; Britton, S.; Gomez, D. Transcription-associated topoisomerase 2α (TOP2A) activity is a major effector of cytotoxicity induced by G-quadruplex ligands. *eLife* **2021**, *10*, e65184.
(32) Rodriguez, R.; Miller, K. M.; Forment, J. V.; Bradshaw, C. R.; Nikan, M.; Britton, S.; Oelschlaegel, T.; Xhemalce, B.; Balasubramanian, S.; Jackson, S. P. Small-molecule-induced DNA damage identifies alternative DNA structures in human genes. *Nat. Chem. Biol.* **2012**, *8*, 301−310.
(33) Bonner, W. M.; Redon, C. E.; Dickey, J. S.; Nakamura, A. J.; Sedelnikova, O. A.; Solier, S.; Pommier, Y. γH2AX and cancer. *Nat. Rev. Cancer* **2008**, *8*, 957.
(34) Rossetto, D.; Avvakumov, N.; Côté, J. Histone phosphorylation. *Epigenetics* **2012**, *7*, 1098−1108.
(35) Rappold, I.; Iwabuchi, K.; Date, T.; Chen, J. Tumor Suppressor P53 Binding Protein 1 (53bp1) Is Involved in DNA Damage−Signaling Pathways. *J. Cell Biol.* **2001**, *153*, 613−620.
(36) Biffi, G.; Tannahill, D.; McCafferty, J.; Balasubramanian, S. Quantitative visualization of DNA G-quadruplex structures in human cells. *Nat. Chem.* **2013**, *5*, 182−186.
(37) François, M.; Leifert, W. R.; Hecker, J.; Faunt, J.; Fenech, M. F. Guanine-quadruplexes are increased in mild cognitive impairment and correlate with cognitive function and chromosomal DNA damage. *DNA Repair* **2016**, *46*, 29−36.
(38) Marchetti, C.; Zyner, K. G.; Ohnmacht, S. A.; Robson, M.; Haider, S. M.; Morton, J. P.; Marsico, G.; Vo, T.; Laughlin-Toth, S.; Ahmed, A. A.; Di Vita, G.; Pazitna, I.; Gunaratnam, M.; Besser, R. J.; Andrade, A. C. G.; Diocou, S.; Pike, J. A.; Tannahill, D.; Pedley, R. B.; Evans, T. R. J.; Wilson, W. D.; Balasubramanian, S.; Neidle, S. Targeting Multiple Effector Pathways in Pancreatic Ductal Adenocarcinoma with a G-Quadruplex-Binding Small Molecule. *J. Med. Chem.* **2018**, *61*, 2500−2517.
(39) Henderson, A.; Wu, Y.; Huang, Y. C.; Chavez, E. A.; Platt, J.; Johnson, F. B.; Brosh, R. M., Jr.; Sen, D.; Lansdorp, P. M. Detection of G-quadruplex DNA in mammalian cells. *Nucleic Acids Res.* **2014**, *42*, 860−869.
(40) Lee, W. T. C.; Yin, Y.; Morten, M. J.; Tonzi, P.; Gwo, P. P.; Odermatt, D. C.; Modesti, M.; Cantor, S. B.; Gari, K.; Huang, T. T.; Rothenberg, E. Single-molecule imaging reveals replication fork coupled formation of G-quadruplex structures hinders local replication stress signaling. *Nat. Commun.* **2021**, *12*, 2525.
(41) Porru, M.; Artuso, S.; Salvati, E.; Bianco, A.; Franceschin, M.; Diodoro, M. G.; Passeri, D.; Orlandi, A.; Savorani, F.; D'Incalci, M.; Biroccio, A.; Leonetti, C. Targeting G-Quadruplex DNA Structures by EMICORON Has a Strong Antitumor Efficacy against Advanced Models of Human Colon Cancer. *Mol. Cancer Ther.* **2015**, *14*, 2541−2551.
(42) Salvati, E.; Doria, F.; Manoli, F.; D'Angelo, C.; Biroccio, A.; Freccero, M.; Manet, I. A bimodal fluorescent and photocytotoxic naphthalene diimide for theranostic applications. *Org. Biomol. Chem.* **2016**, *14*, 7238−7249.

https://doi.org/10.1021/jacsau.2c00082
JACS Au 2022, 2, 1588−1595